JACS
JOURNAL OF THE AMERICAN CHEMICAL SOCIETY
pubs.acs.org/JACS
Article

Inorganic Halide Double Perovskites with Optoelectronic Properties Modulated by Sublattice Mixing

Christopher J. Bartel,* Jacob M. Clary, Christopher Sutton, Derek Vigil-Fowler, Bryan R. Goldsmith, Aaron M. Holder, and Charles B. Musgrave*

Cite This: J. Am. Chem. Soc. 2020, 142, 5135−5145
Read Online
ACCESS | Metrics & More | Article Recommendations | Supporting Information

Downloaded via FRITZ HABER INST DER MPI on March 19, 2020 at 08:50:01 (UTC).
See https://pubs.acs.org/sharingguidelines for options on how to legitimately share published articles.

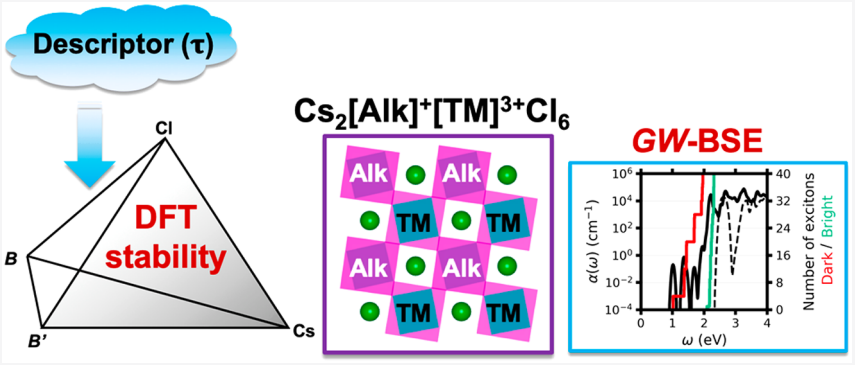

ABSTRACT: All-inorganic halide double perovskites have emerged as a promising class of materials that are potentially more stable and less toxic than lead-containing hybrid organic−inorganic perovskite optoelectronic materials. In this work, 311 cesium chloride double perovskites ($Cs_2BB'Cl_6$) were selected from a set of 903 compounds as likely being stable on the basis of a statistically learned tolerance factor (τ) for perovskite stability. First-principles calculations on these 311 double perovskites were then performed to assess their stability and identify candidates with band gaps appropriate for optoelectronic applications. We predict that 261 of the 311 $Cs_2BB'Cl_6$ compounds are likely synthesizable on the basis of a thermodynamic analysis of their decomposition to competing compounds (decomposition enthalpy <0.05 eV/atom). Of these 261 likely synthesizable compounds, 47 contain no toxic elements and have direct or nearly direct (within 100 meV) band gaps between 1 and 3 eV, as computed with hybrid density functional theory (HSE06). Within this set, we identify the triple-alkali perovskites $Cs_2[Alk]^+[TM]^{3+}Cl_6$, where Alk is a group 1 alkali cation and TM is a transition-metal cation, as a class of $Cs_2BB'Cl_6$ double perovskites with remarkable optical properties, including large and tunable exciton binding energies as computed by the *GW*-Bethe−Salpeter equation (*GW*-BSE) method. We attribute the unusual electronic structure of these compounds to the mixing of the Alk-Cl and TM-Cl sublattices, leading to materials with small band gaps, large exciton binding energies, and absorption spectra that are strongly influenced by the identity of the transition metal. The role of the double-perovskite structure in enabling these unique properties is probed through an analysis of the electronic structures and chemical bonding of these compounds in comparison with other transition-metal and alkali transition-metal halides.

1. INTRODUCTION

Double perovskites ($A_2BB'X_6$) have emerged as high-performance materials for many applications including electrocatalysts,[1] ferroelectrics,[2] white light emitters,[3] phosphors,[4] magnetoresistive materials,[5] and spintronics[6] and as lead-free and all-inorganic alternatives to hybrid organic−inorganic lead halide solar absorbers.[7−11] Motivated by the recent demonstrations of high stability and promising optoelectronic properties of double perovskites with $A = Cs^+$ and $X = Cl^-$ (Figure 1a),[3,4,8,9,11,12] we performed a detailed computational analysis of the $Cs_2BB'Cl_6$ space.

We first enumerated all 903 $Cs_2BB'Cl_6$ formulas composed from 43 possible *B*-site cations and identified 311 compounds with a predicted probability of forming a stable perovskite ($P(\tau)$) >50%, where τ is our recently introduced tolerance factor for perovskite stability (Figure 1b,c).[13] Among these 311 compounds, 4 have been recently synthesized and characterized as potential optoelectronic materials—$Cs_2AgBiCl_6$,[8] $Cs_2AgInCl_6$,[9] $Cs_2AgTlCl_6$,[11] and $Cs_2AgSbCl_6$[12]—and 17 others

Received: November 18, 2019
Published: February 24, 2020

© 2020 American Chemical Society

https://dx.doi.org/10.1021/jacs.9b12440
J. Am. Chem. Soc. 2020, 142, 5135−5145

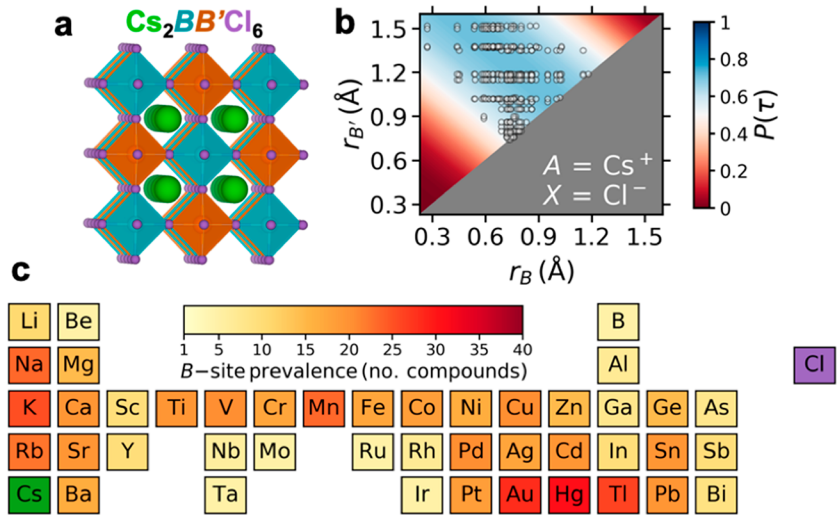

Figure 1. Double-perovskite cesium chlorides. (a) Structure of ideal rock-salt double perovskite where Cs^+ is surrounded by a network of corner-sharing BCl_6 octahedra that alternate between the B and B' cations. (b) The range of ionic radii for the B site (r_B) and B' site ($r_{B'}$) of the 311 $Cs_2BB'Cl_6$ compounds examined in this study with their corresponding τ-derived probability ($P(\tau)$) of forming a stable perovskite structure. (c) Heat map of the occurrence of the 43 elements considered as B or B' cations in this work.

are tabulated in the Inorganic Crystal Structure Database.[14,15] To our knowledge, the remaining 290 compounds have not yet been synthesized and <25% have been assessed computationally with varying levels of detail and theory.[6,7,16−19]

Within the broad composition space of potential $Cs_2BB'Cl_6$ double perovskites, we computed each compound's stability against decomposition into competing compounds and evaluated the effect of structural distortions on the stability and electronic structure. This analysis reveals that it is imperative to allow for structural distortions to accurately model these materials and provide experimentalists with a reliable database of double perovskites and their properties. By parsing this database, we identified triple-alkali perovskites (TAPs) as a new class of stable, small-band-gap semiconductors with tunable absorption profiles that are modulated by the incorporation of alkali cations and transition-metal (TM) cations into the alternating B and B' sites of the double perovskite.

These TAP compounds contain two mixed sublattices composed of octahedra occupied by either TM or alkali cations in their centers and Cl^- anions in their corners. A detailed analysis of a subset of the TAPs using the GW approximation and the Bethe−Salpeter equation (BSE)[20−25] along with a chemical bonding analysis shows that this sublattice mixing gives rise to these materials' remarkable electronic structures and optical properties. Specifically, we find that within this class of compounds are small- to moderate-band-gap semiconductors with large exciton binding energies (as in insulating alkali halides[26]) and dark excitons with energies as low as half of the energy of the onset of absorption (as in transition-metal chlorides[27]), which may have applications in sensing, spintronics, and quantum information storage because of their long coherence lifetimes.[28−31]

2. RESULTS AND DISCUSSION

2.1. Convex Hull Stability Analysis. For each of the 311 $Cs_2BB'Cl_6$ compounds that are predicted to be stable as perovskites using τ, we calculated the decomposition enthalpy,[32] ΔH_d, which is the enthalpy relative to all possible competing compounds, by constructing the quaternary convex hull phase diagrams using the formation enthalpy of the compound relative to its elemental phases, ΔH_f, for all compounds that belong to the Cs−Cl, B−Cl, B'−Cl, Cs−B−Cl, Cs−B'−Cl, and B−B'−Cl chemical spaces that are available on the Materials Project.[33] The formation enthalpies, ΔH_f, were computed using density functional theory (DFT) with the SCAN exchange-correlation functional.[34] The decomposition enthalpy was used herein and not the Gibbs energy of decomposition because the synthesis of halide perovskites is often performed near room temperature where the 0 K enthalpy of solid-state compounds is a good, and less computationally demanding, approximation for the thermodynamic driving force for stability.[35]

We note that 82% of the decomposition reactions that define the stability of the 311 double perovskites include ternary phases (e.g., the decomposition reaction of $Cs_2AgAuCl_6$ includes $CsAgCl_2$ but not AgCl), emphasizing the importance of including compounds beyond the common binary compounds and elemental phases used as synthetic precursors when assessing the stability of quaternary materials.[18,19,36] Consequently, ΔH_f is not a good predictor of stability because it considers only decomposition into elemental phases. Indeed, effectively no linear correlation exists between ΔH_d and ΔH_f (R^2 = 0.03), which demonstrates the importance of determining stability by calculating ΔH_d from the convex hull of formation enthalpies in the screening of new materials.

Of the 311 (49%) $Cs_2BB'Cl_6$ compounds predicted to be stable perovskites by τ, 152 are confirmed as stable ($\Delta H_d < 0$) using SCAN. Another 109 $Cs_2BB'Cl_6$ compounds (35%) fall within the thermodynamic window ($0 \le \Delta H_d \le 0.05$ eV/atom) where accessible metastable phases are often found.[37] Notably, 21 $Cs_2BB'Cl_6$ compounds have been synthesized, with 20 also satisfying $\Delta H_d < 0$ and Cs_2KBiCl_6 being only minimally metastable with ΔH_d = +0.006 eV/atom.

These results provide quantitative support for the predictive power of τ-derived perovskite stabilities over a wide range of double-perovskite compositions despite τ being trained exclusively using single-perovskite stabilities. However, the 84% agreement between τ and DFT-computed ΔH_d values of the $Cs_2BB'Cl_6$ compounds is lower than the 92% accuracy in the prediction of stable ABX_3 materials in comparison with

https://dx.doi.org/10.1021/jacs.9b12440
J. Am. Chem. Soc. 2020, 142, 5135−5145

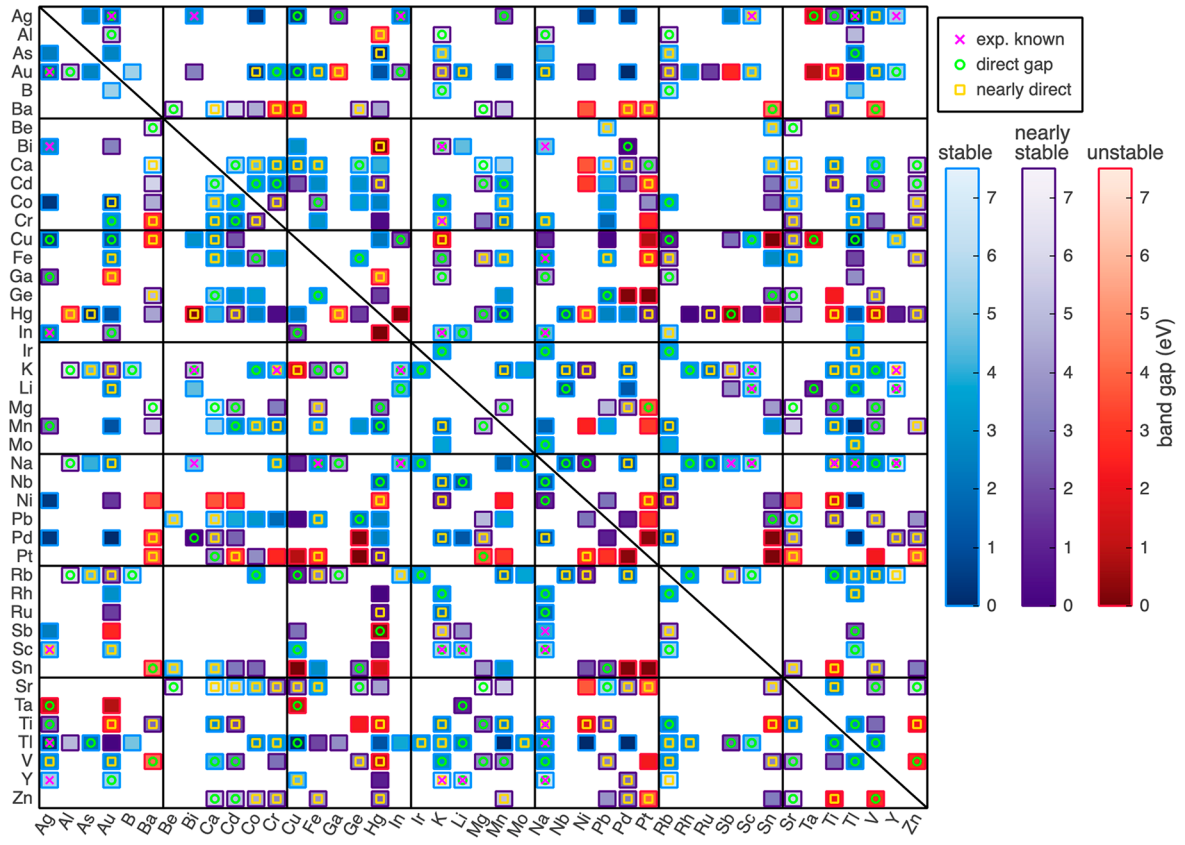

Figure 2. Map of $Cs_2BB'Cl_6$ properties. B and B' are defined along each axis (note that B and B' are treated equivalently in this work; therefore, the data are mirrored across the diagonal line). Stable compounds ($\Delta H_d \leq 0$ eV/atom) are shown in blue, nearly stable compounds ($0 < \Delta H_d \leq 0.05$ eV/atom) are shown in purple, and unstable compounds are shown in red ($\Delta H_d > 0.05$ eV/atom), where ΔH_d is calculated with SCAN. The color intensity of each compound corresponds to the band gap calculated using single-point HSE06 at the SCAN-optimized geometry (spHSE06@SCAN). Compounds that have direct band gaps are indicated with an open green circle. Compounds that have indirect gaps that are within 100 meV of the direct gap are indicated with an open gold square. Compounds that have been reported experimentally are indicated with a pink ×. An interactive version of this plot that assists with navigation and displays additional properties is available in the Supporting Information.

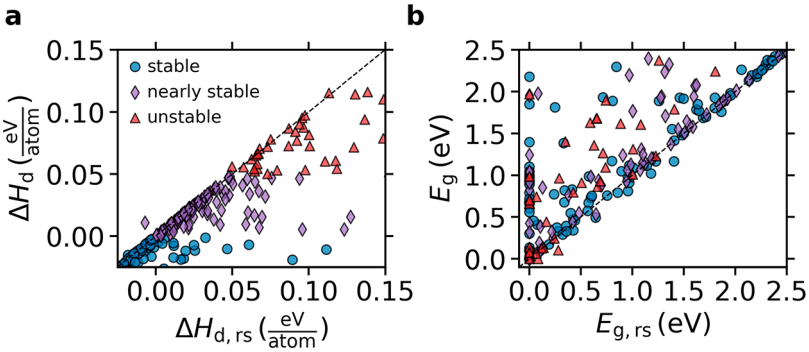

Figure 3. Distortion effects on double-perovskite properties. (a) Effect of structural distortions on thermodynamic stability. The subscript rs indicates preassignment in the high-symmetry rock-salt crystal structure. (b) Effect of structural distortions on the band gap. In each panel, blue circles indicate stable compounds ($\Delta H_d \leq 0$ eV/atom), purple pentagons indicate nearly stable compounds ($0 < \Delta H_d \leq 0.05$ eV/atom), and red triangles indicate unstable compounds ($\Delta H_d > 0.05$ eV/atom). The SCAN functional was used to calculate all quantities reported in this figure. The ranges of ΔH_d and E_g have been restricted to highlight the effect of distortions.

experiment reported in ref 13. We attribute this to the averaging of the B and B' radii (r_B and $r_{B'}$) into a single effective radius r_B for the calculation of τ for double perovskites and the relatively conservative threshold chosen to indicate maximum metastability to be synthesizable as a perovskite ($\Delta H_d \leq 0.05$ eV/atom).[13]

Although all-inorganic halide double perovskites have received considerable attention in recent years, we emphasize that this composition space provides ample opportunity for future device tunability as a result of the wide range (~6 eV) of computed band gaps, E_g, spanned by these compounds (Figure 2). Of the 261 $Cs_2BB'Cl_6$ compounds that are likely synthesizable (based on $\Delta H_d \leq 0.05$ eV/atom), 97 exhibit a band gap energy between 1 and 3 eV—as computed with the hybrid functional, HSE06,[38] at the SCAN geometry (spHSE06@SCAN)—that makes them potentially suitable as materials for a range of optoelectronic[39,40] or photocatalytic[41]

https://dx.doi.org/10.1021/jacs.9b12440
J. Am. Chem. Soc. 2020, 142, 5135−5145

applications, and of these, only 6 have been synthesized to date. Beyond the computed values of E_g and ΔH_d of the 261 $Cs_2BB'Cl_6$ compounds displayed in Figure 2, a number of additional properties are reported through an interactive version of Figure 2 and Table S1 available in the Supporting Information.

2.2. Effects of Distortion. Structural distortions play a prominent role in defining the stability and properties of perovskites and can arise from the presence of Jahn−Teller ions (e.g., Cu^{2+} or Mn^{3+}),[42] ferroelectric displacements,[43] and cation size mismatch.[44] Nevertheless, researchers often assume the high-symmetry cubic rock salt structure when they perform high-throughput computational screening of new perovskite oxides and halides.[17,45−48] Recent studies have shown that this assumption can lead to incorrect predictions of thermodynamic stability[13,49] and electronic structure[50] for single perovskites, ABX_3. The influence of structural distortions on the properties of halide double perovskites has not previously been analyzed. To quantify the effect of these distortions, we repeated our stability analysis for the same 311 $Cs_2BB'Cl_6$ compounds but now constrained in the ideal, high-symmetry cubic rock salt structure, rs (see Methods for additional details) and computed the effect of this approximation on their stability (Figure 3a) and band gap (Figure 3b). Of the 311 compounds, 24 compounds with $\Delta H_d \geq 0$ in the rs structure become thermodynamically stable ($\Delta H_d < 0$) upon distortion, which on average lowered the energy relative to the *rs* structure by 0.02 eV/atom. The effect of structural distortions on band gap is even more pronounced, where the average E_g computed with SCAN increases by 0.35 eV upon distortion. In fact, 45 of the 55 metallic rs structures become semiconductors upon relaxation into their lower energy distorted structures, resulting in an average band gap of 0.76 eV in the fully relaxed structures for these metallic rs structures and lowering the percentage of metallic compounds from 18% to 3% of the 311 compounds. Because SCAN underestimates band gaps relative to experiment,[51] we expect that the gap-opening effect of the SCAN-predicted distortions is underestimated. A few representative examples of the distortion effect on the electronic structure (or lack thereof) are depicted in Figure S2.

2.3. Potential Optoelectronic Materials. All-inorganic halide double perovskites present an alternative to hybrid organic−inorganic perovskite semiconductors containing Pb, but the realization of these materials has been so far limited to only a handful of compounds. The $Cs_2BB'Cl_6$ space was chosen for this study on the basis of several compositional trends. Cs^+ enables the greatest opportunity for stabilizing inorganic perovskite structures with large *X* sites (e.g., Cl^-, Br^-, I^-) because it is the largest inorganic cation, and increasing r_A widens the range of potential *B*-site cations that can form stable perovskites.[13] Band gaps typically decrease to optically relevant values as r_X increases,[52] but the minimum r_B to form BX_6 octahedra increases with r_X, thereby limiting potential *B*-site cations to larger and larger ions as the anion becomes larger. By analyzing the wide range of 311 B/B' combinations within the $Cs_2BB'Cl_6$ double-perovskite structure, we predict that 47 (meta)stable materials exhibit a band gap suitable for potential application as the active materials in optoelectronic devices. These 47 materials were identified on the basis of the following criteria: (1) $\Delta H_d \leq 0.05$ eV/atom (29 of 47 compounds are stable with $\Delta H_d < 0$ eV/atom), (2) $1 \leq E_g \leq 3$ eV as calculated by spHSE06@SCAN, (3) direct gaps or indirect gaps ≤100 meV lower than the direct gap (12 of 47 compounds exhibit direct gaps), and (4) the absence of toxic and radioactive elements (Figure 4). We find that spHSE06@SCAN produces band gaps ∼1.1 eV larger on average than SCAN for the

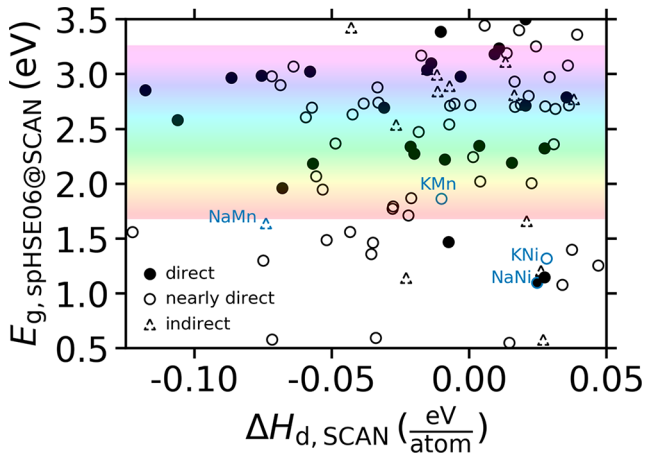

Figure 4. Stable, small-band-gap halide perovskites. HSE06-calculated band gaps of SCAN-optimized structures ($E_{g,spHSE06@SCAN}$) and computed stability of each material ($\Delta H_{d,SCAN}$). The nature of the band gap is indicated by the marker—filled markers indicate direct band gaps, open markers indicate indirect gaps ≤100 meV lower than the direct gap, and open triangular markers with dashed borders indicate indirect gaps >100 meV lower than the direct gap. The visible spectrum is overlaid for context. The data are restricted to band gaps that align with most of the solar spectrum (0.5−3.5 eV). Data points for four $Cs_2(K,Na)(Mn,Ni)Cl_6$ compounds are labeled that are discussed in detail in the text and figures.

perovskites in this data set (Figure S3). This down-selection procedure rediscovers $Cs_2AgInCl_6$, which was recently shown to exhibit stable emission of white light when it is alloyed with Na^+ on the *B* site.[3] Interestingly, alkali (group 1) cations also occupy the *B* sites of 26 of these 47 materials, which we henceforth refer to as triple-alkali perovskites (TAPs). While these compounds have received little attention to date, we show that they have unique and tunable optical properties, enabled by the ionic stabilization of oxidized transition metals by the alkali halide octahedra of the double-perovskite structure.

2.4. Excitons in Triple-Alkali Perovskites. The 26 stable TAPs that meet the above stability and band gap criteria were found to exhibit qualitatively similar electronic structures, having narrow valence and conduction bands with band edges comprised of primarily TM d and Cl p character (see Figure S4 for a representative example (Cs_2KMnCl_6) of the *GW* band structure and projected density of states (DOS)), indicating that these frontier orbitals do not overlap significantly with orbitals localized on neighboring atoms. However, the dominant orbital character does depend to some extent on the $B−B'$ combination (Table S2). The minimally dispersive conduction bands in these compounds result in a low electronic dimensionality[53] and indicate that their excited electrons have high effective masses, which likely precludes their application in devices requiring fast charge carrier mobility (e.g., solar absorbers). Nevertheless, we applied state of the art many-body GW_0 and BSE calculations to further characterize the unique electronic structure of four compounds within this class—$Cs_2(K,Na)(Mn,Ni)Cl_6$—as a characteristic subset of this new group of stable, small- to moderate-band-gap perovskites. This group was chosen to understand the effects of alkali and TM swapping within the general $Cs_2[Alk]^+[TM]^{3+}Cl_6$ TAP formula. Because the TM atom in perovskites resides within an octahedral crystal field, its

https://dx.doi.org/10.1021/jacs.9b12440
J. Am. Chem. Soc. 2020, 142, 5135−5145

Table 1. PBE and GW_0 Computed Direct and Fundamental Band Gaps for the Four $Cs_2(K,Na)(Mn,Ni)Cl_6$ Perovskites Analyzed in This Work Using the *GW*-BSE Methodology[a]

		$E_{g,PBE}$ (eV)		$E_{g,GW0}$ (eV)		
B-*B*′ combination	spin state	fundamental	direct	fundamental	direct	$E_{b,xct\text{-}bright}$ [$E_{b,xct\text{-}dark}$] (eV)
Na−Mn	AFM1	0.59	0.62	2.69	2.69	0.31 [1.43]
	AFM2	0.42	0.45	2.96	2.96	0.35 [1.69]
K−Mn	AFM1	0.52	0.64	3.30	3.42	1.04 [2.05]
	AFM2	0.45	0.65	3.30	3.50	0.43 [2.03]
Na−Ni	AFM1	0.36	0.55	1.78	1.78	0.22 [0.65]
	AFM2	0.20	0.56	2.08	2.09	0.28 [0.95]
K−Ni	AFM1	0.30	0.50	2.44	2.54	0.49 [1.42]
	AFM2	0.20	0.50	2.48	2.75	0.71 [1.48]

[a]The exciton binding energies $E_{b,xct\text{-}bright}$ and $E_{b,xct\text{-}dark}$ are shown in the rightmost column. $E_{b,xct\text{-}bright}$ is defined as the difference between $E_{g,GW0}$ and the energy at which $\alpha > 10$. $E_{b,xct\text{-}dark}$ is defined as the difference between $E_{g,GW0}$ and the energy of the first dark exciton.

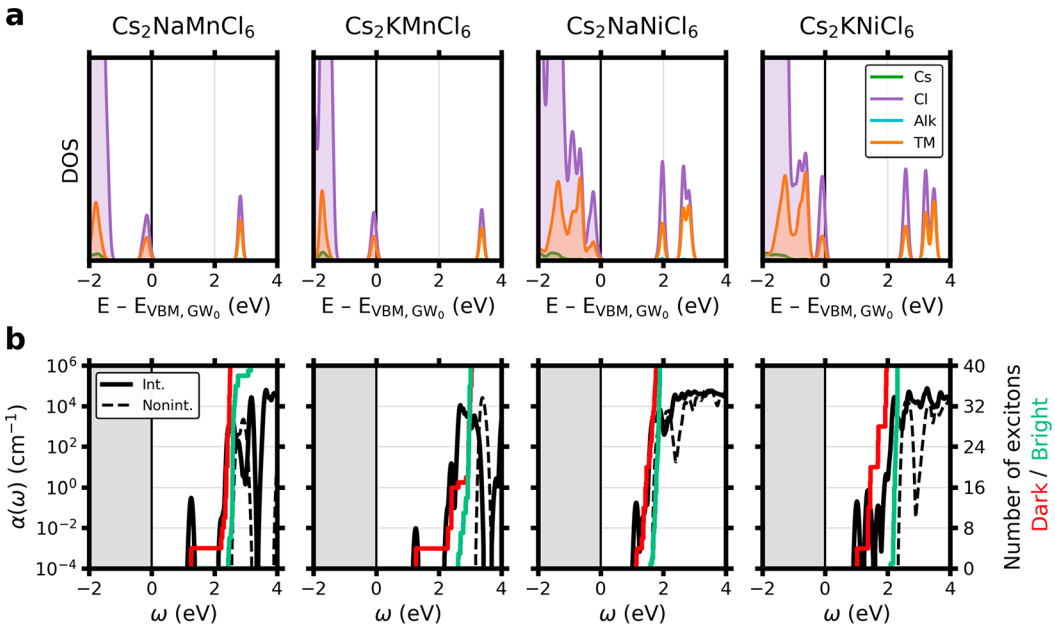

Figure 5. GW_0 electronic structure and BSE optical properties of $Cs_2(K,Na)(Mn,Ni)Cl_6$. (a) Density of states computed using GW_0 of the four $Cs_2(K,Na)(Mn,Ni)Cl_6$ perovskites in their AFM1 spin configuration projected onto each atomic species with the GW_0 VBM set to zero. (b) BSE absorption coefficient (α) with (solid lines) and without (dashed line) electron−hole interactions and the cumulative number of dark and bright excitons over increasing energy.

d orbitals split with the t_{2g} orbitals (d_{xy}, d_{yz}, d_{xy}) lying lower in energy and the e_g orbitals (d_{z^2} and $d_{x^2-y^2}$) higher in energy. Therefore, the degree of filling of the d shell, and consequently the electronic structure, directly depends on the choice of the TM atom. For example, both Mn (Ni)-containing compounds exhibit unoccupied (occupied) states with primarily Mn (Ni) t_{2g} orbital character at approximately 5 (−1) eV and exhibit no states at −1 (5) eV.

GW_0 opens the computed band gap in comparison to the generalized gradient approximation (PBE)[54] by approximately 2−3 eV for all four compounds (Table 1, Figure 5, and Figure S5), but all are still predicted to have relatively small band gaps ($E_{g,GW0} \lesssim 3.3$ eV, Figure 5) in comparison with other ionic halides (e.g., NaCl). These gaps are calculated for two different antiferromagnetic spin states (AFM1 and AFM2, Figure S6) because of the low total energy difference of <1 meV/atom among all unique spin configurations. Additionally, for each material, the spin configurations resulted in qualitatively similar band structures with band gaps that differed by 0.3 eV or less.

The inclusion of electron/hole interactions within the BSE formalism qualitatively changes the absorption spectra and shifts the onsets of absorption to much lower energies (Figure 5). These materials are all predicted to have large exciton binding energies, $E_{b,xct\text{-}bright}$, with $0.22 \leq E_{b,xct\text{-}bright} \leq 1.04$ eV (Table 1), where $E_{b,xct\text{-}bright}$ is defined as the difference between $E_{g,GW0}$ and the energy of the first state at which the absorption coefficient α is >10. These large binding energies are extraordinary in that they occur in moderate-band-gap 3D (geometrically periodic in all three spatial dimensions) crystalline solids and are comparable to or exceed those reported for 2D transition-metal dichalcogenides,[55] layered hybrid halide perovskites,[56] and wide-band-gap (E_g > 6 eV) inorganic bulk crystals.[57] Excitons that are strongly bound (hundreds of meV) and optically accessible (band gap $\lesssim$4 eV) have historically been limited only to 2D materials such as transition-metal dichalcogenides.[31] Here we show that this phenomenon can be extended to 3D double perovskites, which, unlike transition-metal dichalcogenides, are stable across a wide range of compositions. This compositional flexibility allows for careful

https://dx.doi.org/10.1021/jacs.9b12440
J. Am. Chem. Soc. 2020, 142, 5135−5145

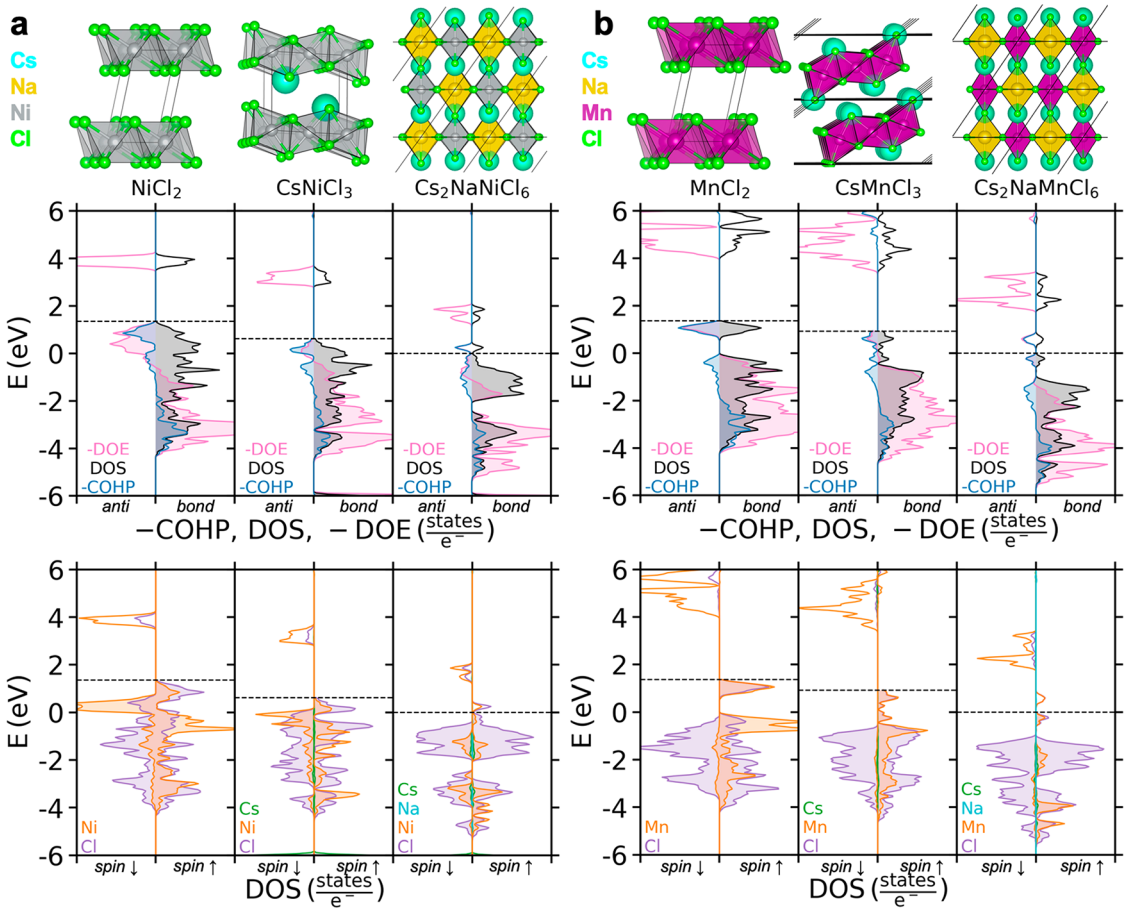

Figure 6. Evolution of the properties of the $Cs_2Na(Mn,Ni)Cl_6$ triple-alkali perovskites with composition. Geometries, DOS, COHP, DOE, and element-projected DOS for (a) $NiCl_2$, $CsNiCl_3$, and $Cs_2NaNiCl_6$ and (b) $MnCl_2$, $CsMnCl_3$, and $Cs_2NaMnCl_6$. The compounds shown in each panel were chosen to highlight the consequences of incorporating a third alkali cation into the double-perovskite structure. In each panel, the dashed line corresponds to the core-level aligned Fermi level (with zero being the TAP Fermi level).

tuning of optical properties and also suggests the prevalence of many more stable compounds having these properties that have yet to be discovered. We note that, because of the small energy difference between the AFM1 and AFM2 spin configurations, we expect that both configurations will be present at ambient temperature and lower (raise) the maximum (minimum) achievable $E_{b,xct}$ for each material.

For all four materials, the lowest energy excitons are dark, occur at much lower energies than the first bright excitons, and involve transitions between the two highest energy valence bands and two lowest energy conduction bands. These excitons are delocalized across multiple neighboring $TMCl_6$ octahedra, consistent with the delocalization that occurs for $NiCl_2$ (taking into account the added $AlkCl_6$ octahedra in our double-perovskite structure).[27] Furthermore, the features present in the absorption spectra and the profiles of the cumulative numbers of excitons are also strongly influenced by the choice of TM. For example, Figure 5b shows that the Mn-containing compounds both exhibit small isolated peaks in their absorption spectra near 1.2 eV, whereas the Ni-containing compounds both exhibit a small shoulder near 1.3−1.4 eV in their absorption spectra prior to the onset of absorption. For the Ni-containing compounds, the dark excitons at 1.3−1.4 eV involve transitions from valence states with energies 0.1−1.1 eV below the two highest energy valence states to conduction states with energies 0.1−1.0 eV above the two lowest energy conduction states. In contrast, many of the dark excitons at 2.3−2.4 eV for the Mn-containing compounds involve transitions from valence states 1.0−1.8 eV lower in energy than the two highest energy valence bands to the two lowest energy conduction states. Therefore, for Ni-containing compounds, the presence of occupied states with Cl p and Ni d character immediately below the VBM is reflected in their absorption spectra.

2.5. Origins of Triple-Alkali Perovskite Stability. The electronic structure and exciton physics of the $Cs_2(K,Na)(Mn,Ni)Cl_6$ TAP materials appear to be an intriguing combination of the two simpler material classes that occupy the two double-perovskite sublattices—alkali halides and transition-metal halides. In three-dimensional solids, the largest known exciton binding energies of ∼0.7−1.5 eV occur in wide-band-gap halides such as NaCl, KCl, LiCl, and LiF.[26,58] Furthermore, TM halides (such as $NiCl_2$) are known to produce dark excitons with large binding energies.[27] The band structures of the $Cs_2(K,Na)(Mn,Ni)Cl_6$ perovskites resemble those of both the cubic alkali halides and TM halides. For instance, the band edge states of NaCl, CsCl, and the $Cs_2(K,Na)(Mn,Ni)Cl_6$ TAPs all exhibit strong Cl character. In addition, the $Cs_2(K,Na)(Mn,Ni)Cl_6$ perovskites have hybridized unoccupied states with alkali−Cl s−p character at energies relative to their valence band maximum (VBM) similar to the band gaps of pure alkali halides (i.e., >6 eV relative to the VBM). As in $MnCl_2$ and $NiCl_2$, both the valence and conduction band edge states of the

https://dx.doi.org/10.1021/jacs.9b12440
J. Am. Chem. Soc. 2020, 142, 5135−5145

$Cs_2(K,Na)(Mn,Ni)Cl_6$ TAPs are composed of hybridized TM−Cl d−p states that exhibit minimal dispersion. We expect that the exciton transport and localization properties of these compounds will be influenced by exchange interactions determined by their spin configuration as in magnetic TM halides.[59]

While the underlying electronic structures of the TAPs resemble those of a mixture of the binary alkali and transition-metal halides, this picture does not explain why TAPs are stable with respect to decomposition into these and other competing phases. To understand the origins of TAP stability, we characterize the evolution of the electronic DOS, crystal orbital Hamilton populations (COHPs),[60] and density of energy (DOE)[61] from the binary TM chloride ($TMCl_2$) by incorporating Cs^+ to form $CsTMCl_3$ and then the alkali to form the TAP—$Cs_2AlkTMCl_6$. This comparison is shown for Alk = Na in Figure 6 and for Alk = K in Figure S7 (TM = Ni in panel a and TM = Mn in panel b of each figure).

The TM chlorides, $NiCl_2$ and $MnCl_2$, are two-dimensional materials comprised of face-sharing $TMCl_6$ octahedra that form layers with an interlayer spacing of ∼3.9 Å. These compounds have wide band gaps ($E_{g,SCAN}$ = 3.5−4 eV) that arise from majority Cl p to majority TM d transitions. The occupied states at the Fermi level possess a large degree of TM−Cl antibonding character (−COHP < 0) that arises from the face-sharing nature of the $TMCl_6$ octahedra. The states at the conduction band minima are nonbonding (−COHP = 0).

These same features are present in the corresponding $CsTMCl_3$ compounds, which exhibit similar layers of face-sharing $TMCl_6$ octahedra but are now separated by large Cs^+ cations instead of interstitial space. Coulombic interactions with Cs^+ ionically stabilize the $TMCl_6$ octahedra, slightly diminishing the antibonding character of states at the Fermi energy and lowering the energy of all states. These materials still have large band gaps and the same transitions from Cl p (antibonding) to TM d (nonbonding) states.

When an alkali cation is substituted into the octahedra of the TAP double perovskites, the chemistry and structure change dramatically (Figure 6). The $TMCl_6$ octahedra become corner sharing, the TM cations are nominally oxidized from 2+ to 3+, and the band gaps are lowered. Further oxidation of the TM cations leads to a splitting of the $TMCl_2$/$CsTMCl_3$ valence band states into the low-lying conduction band states of the TAPs, shifting the TM−Cl antibonding states to energies above the Fermi level and lowering the energies of occupied states of the TAPs. The presence of $AlkCl_6$ octahedra in the double-perovskite structure ionically stabilizes the more oxidized TM atoms in corner-sharing octahedra, as is evident from the destabilizing −DOE < 0 states at the Fermi level in $TMCl_2$ and $CsTMCl_3$ that vanish in both TAPs. This is further supported by the general increase in the Bader charge[62] of the TM cations and decrease in electrostatic energy for TAPs in comparison with $TMCl_2$/$CsTMCl_3$ (Table S3).

The variability in optoelectronic properties within the four TAPs shown in Figure 5 suggests that ample opportunity exists to tune optical phenomena by alloying on either *B* site within this sublattice-mixed double-perovskite framework. Tuning may be accomplished by complete or partial TM or alkali substitutions, thin-film growth, lattice straining, TM spin coupling via application of a magnetic field, or variation of the temperature. Indeed, we find that, even within the class of four materials studied in Figure 5, exchanging K for Na or Ni for Mn noticeably shifts the band gap and absorption spectra. As a result, our stability screening of this class of compounds likely contains many compounds worthy of further investigation, including for applications beyond the optoelectronic applications we examined in detail for the four TAP materials. For example, recent work has shown that $Cs_2Ge(Mn,V,Ni)Cl_6$ exhibit desirable properties for spintronics including intrinsic ferromagnetism, large spin splitting, and a high Curie temperature.[6] Modulation of the optical properties of layered hybrid perovskites has received considerable interest in recent years,[56] and our results suggest that this class of triple-alkali 3D perovskite semiconductors comprised of earth-abundant and nontoxic elements warrants further study for a range of optical and electronic applications.

3. CONCLUSIONS

We identified 311 cesium chloride double perovskites ($Cs_2BB'Cl_6$) from a set of 903 compounds to likely form as perovskites using the recently introduced tolerance factor, τ. The thermodynamic stability of each of these 311 compounds was determined by calculating their enthalpies of decomposition, ΔH_d, into elemental, binary, and ternary phases using DFT and the SCAN functional. The role of distortions was quantified for the 311 likely stable compounds by comparing symmetry-broken, relaxed structures to those constrained to the ideal rock-salt symmetry. On average, these distortions lower ΔH_d by 0.02 eV/atom and increase E_g by 0.35 eV. Of the 311 perovskites, 152 are predicted to be stable ($\Delta H_d \leq 0$), and 109 additional perovskites are nearly stable with $0 < \Delta H_d \leq 0.05$ eV/atom and might be realized as persistent metastable phases.

Within the predicted set of stable or nearly stable perovskites, we identified "triple-alkali" perovskites of the form $Cs_2[alkali]^+[transition\ metal]^{3+}Cl_6$ as a new class of stable, small-band-gap perovskites with remarkable optical properties that are attributed to the mixing of alkali and transition-metal halide sublattices. A subset of these materials is shown to have large exciton binding energies of magnitudes similar to those of layered materials and insulating bulk materials even though these are 3D bulk semiconductors with $E_{g,GW0} \leq 3.3$ eV. Furthermore, these properties are shown to be directly related to the $B-B'$ element combination, suggesting that they are highly tunable. We suggest that future studies aim to synthesize and better understand these materials to realize the control of their unique optical phenomena and application in next-generation optoelectronic devices such as room-temperature excitonic devices. This work demonstrates the potential for realization of new all inorganic halide double perovskites with tunable optoelectronic properties by leveraging this concept of sublattice mixing.

4. METHODS

All structures were optimized using the Vienna ab initio simulation package[63,64] with the projector augmented wave method[65,66] and the strongly constrained and appropriately normed (SCAN) meta-GGA density functional,[34] a plane wave energy cutoff of 520 eV, a Γ-centered Monkhorst−Pack *k*-point grid with $20|b_i|$ discretizations along each reciprocal lattice vector, b_i, and high-spin ferromagnetic spin configurations unless otherwise reported. The energy cutoff, *k*-point grid density, and related convergence settings were sufficient to achieve a total energy convergence of <5 meV/atom for all calculations. Rock salt perovskite structures, rs, were optimized from an ideal $Fm\bar{3}m$ unit cell. Distorted structures were obtained by generating a 1×1×2 supercell of the rs structure and randomly displacing all atoms in the cell by 0.1 Å. These distorted structures were used for all analyses that do not include the subscript rs (i.e., to determine stability and band gaps).

https://dx.doi.org/10.1021/jacs.9b12440
J. Am. Chem. Soc. 2020, 142, 5135−5145

A single-point HSE06 calculation was performed at the SCAN-optimized geometries (spHSE06@SCAN) by fixing the cell shape, volume, and atomic positions while the electronic structure was optimized self-consistently until the total energy changed by $<10^{-6}$ eV/cell.

All *GW*-BSE[20−25] calculations were performed on self-consistent geometries optimized with the Perdew−Burke−Ernzerhof[64] (PBE) generalized-gradient approximation functional in the Quantum ESPRESSO code.[67,68] Quantum ESPRESSO is not currently capable of relaxing these spin-polarized structures using the SCAN functional. However, we found that PBE does not change the qualitative electronic structures of these materials and still predicts them to be small-band-gap semiconductors. Thus, we expect that self-consistent GW_0 eigenvalues accurately reflect these materials' actual band gaps. The *GW*-BSE methodology has been shown to yield results in excellent agreement with experiment for a variety of systems,[58] including halide perovskites.[3,11] The mean-field wave function was calculated with multiple-projector pseudopotentials from the SG15 library[69,70] and a 60 Ryd planewave cutoff. The *GW*-BSE calculations were then executed within the BerkeleyGW package.[22,58,71] The dielectric matrix and self-energy were calculated using a 2×2×2 sampling of the supercell Brillouin zone. The total number of bands included was 20× the number of occupied states, and the static remainder[72] was used in the self-energy calculations to accelerate convergence. A 10 Ryd screened Coulomb cutoff was employed. The Hybertsen−Louie generalized plasmon pole model[22] was used to account for the frequency dependence of the inverse dielectric matrix. The quasiparticle gap at the Γ point was converged to within 0.2 eV with respect to the number of bands used to calculate the dielectric matrix and self-energy, screened Coulomb cutoff, supercell sampling, and iterations in *G*. Self-consistent quasiparticle eigenvalues were obtained following one additional iteration in *G* beyond G_0W_0 (GW_0). The band structure paths through *k* space were determined by the Seek-path Python library.[73]

For the *GW*-BSE calculations, the BSE Hamiltonian was first computed using a 2×2×2 Brillouin zone sampling and interpolated onto a 4×4×4 sampling grid.[58] The number of bands on the coarse grid was chosen to converge up to 2 eV above the onset of absorption. This procedure resulted in 70/22 (98/12) valence/conduction bands used for the coarser grid and 35/11 (50/6) valence/conduction bands used for the finer grid for the Mn (Ni)-containing compounds. Doubling the number of conduction bands summed over for both grids did not change the exciton binding energy.

All compounds were optimized as ordered structures with an alternating arrangement of BCl_6 and $B'Cl_6$ octahedra. This structure was used for all property calculations because it has been shown to be the lowest energy[74] and experimentally observed arrangement, except in rare cases.[75] To validate this assumption, we sampled additional arrangements for the four compounds studied with *GW*. From the 80-atom $Cs_{16}Alk_8TM_8Cl_{48}$ supercells with alternating $AlkCl_6$ and $TMCl_6$ octahedra, we generated 18−50 low electrostatic energy structures for each compound with 0−50% Cs/Alk and 0−50% Alk/TM site disorder and calculated their energy using PBE. For all four compounds, we found the lowest energy arrangement to be that with 0% Cs/Alk site disorder and 0% Alk/TM site disorder, thus supporting our use of the alternating arrangement throughout the work. Electrostatic energies were calculated using the Ewald approach as implemented in Pymatgen.[76] COHP and DOE analysis was performed using the LOBSTER code.[77]

■ ASSOCIATED CONTENT

Supporting Information

The Supporting Information is available free of charge at https://pubs.acs.org/doi/10.1021/jacs.9b12440.

Geometric and electronic effects of symmetry-lowering distortions for three compounds, effect of single-point HSE06 on calculated band gaps, band structure and density of states for Cs_2KMnCl_6 at the GW_0 level, antiferromagnetic spin configurations using GW_0 density of states and BSE optical properties for $Cs_2(K,Na)(Mn,Ni)Cl_6$ compounds using alternative spin configurations, structure and chemistry of K-containing triple-alkali perovskites, calculated results for all compounds, electronic structure properties for triple-alkali perovskites, and Bader charge and electrostatic energies for four $Cs_2(K,Na)(Mn,Ni)Cl_6$ compounds (PDF)

SCAN-optimized structures (.cif) for all 311 compounds (ZIP)

Interactive version of Figure 2 (ZIP)

Stabilities and band gaps for all compounds (TXT)

■ AUTHOR INFORMATION

Corresponding Authors

Christopher J. Bartel − *Department of Chemical and Biological Engineering, University of Colorado Boulder, Boulder, Colorado 80309, United States;* orcid.org/0000-0002-5198-5036; Email: christopher.bartel@colorado.edu

Charles B. Musgrave − *Department of Chemical and Biological Engineering, Department of Chemistry, Renewable and Sustainable Energy Institute, and Materials Science and Engineering Program, University of Colorado Boulder, Boulder, Colorado 80309, United States; Materials and Chemical Science and Technology Center, National Renewable Energy Laboratory, Golden, Colorado 80401, United States;* orcid.org/0000-0002-5732-3180; Email: charles.musgrave@colorado.edu

Authors

Jacob M. Clary − *Department of Chemical and Biological Engineering, University of Colorado Boulder, Boulder, Colorado 80309, United States;* orcid.org/0000-0002-6144-759X

Christopher Sutton − *Fritz-Haber-Institut der Max-Planck-Gesellschaft, D-14195 Berlin, Germany*

Derek Vigil-Fowler − *Materials and Chemical Science and Technology Center, National Renewable Energy Laboratory, Golden, Colorado 80401, United States*

Bryan R. Goldsmith − *Department of Chemical Engineering, University of Michigan, Ann Arbor, Michigan 48109, United States;* orcid.org/0000-0003-1264-8018

Aaron M. Holder − *Department of Chemical and Biological Engineering, University of Colorado Boulder, Boulder, Colorado 80309, United States; Materials and Chemical Science and Technology Center, National Renewable Energy Laboratory, Golden, Colorado 80401, United States;* orcid.org/0000-0002-1878-1541

Complete contact information is available at: https://pubs.acs.org/10.1021/jacs.9b12440

Notes

The authors declare no competing financial interest.

■ ACKNOWLEDGMENTS

C.J.B., J.M.C., and C.B.M. acknowledge support from The DOE Fuel Cells and Technology Office HydroGen program award number EERE DE-EE0008088, NSF CHEM 1800592, and NSF CBET 1806079. C.S. acknowledges support from the Alexander von Humboldt fellowship program. D.V.-F. and A.M.H. gratefully acknowledge support from NREL's Laboratory Directed Research and Development (LDRD) program for performing simulations of halide perovskites using beyond-DFT methods. B.R.G. acknowledges Assistant Professor startup funds from the University of Michigan. High-performance computing

https://dx.doi.org/10.1021/jacs.9b12440
J. Am. Chem. Soc. 2020, 142, 5135−5145

resources were sponsored by the U.S. Department of Energy's Office of Energy Efficiency and Renewable Energy, located at NREL.

REFERENCES

(1) Duan, C.; Tong, J.; Shang, M.; Nikodemski, S.; Sanders, M.; Ricote, S.; Almonsoori, A.; O'Hayre, R. Readily Processed Protonic Ceramic Fuel Cells with High Performance at Low Temperatures. *Science* **2015**, *349* (6254), 1321−1326.
(2) Li, Z.; Cho, Y.; Li, X.; Li, X.; Aimi, A.; Inaguma, Y.; Alonso, J. A.; Fernandez-Diaz, M. T.; Yan, J.; Downer, M. C.; Henkelman, G.; Goodenough, J. B.; Zhou, J. New Mechanism for Ferroelectricity in the Perovskite Ca2−XMnxTi2O6 Synthesized by Spark Plasma Sintering. *J. Am. Chem. Soc.* **2018**, *140* (6), 2214−2220.
(3) Luo, J.; Wang, X.; Li, S.; Liu, J.; Guo, Y.; Niu, G.; Yao, L.; Fu, Y.; Gao, L.; Dong, Q.; Zhao, C.; Leng, M.; Ma, F.; Liang, W.; Wang, L.; Jin, S.; Han, J.; Zhang, L.; Etheridge, J.; Wang, J.; Yan, Y.; Sargent, E. H.; Tang, J. Efficient and Stable Emission of Warm-White Light from Lead-Free Halide Double Perovskites. *Nature* **2018**, *563* (7732), 541−545.
(4) Majher, J. D.; Gray, M. B.; Strom, T. A.; Woodward, P. M. Cs2NaBiCl6:Mn2+—A New Orange-Red Halide Double Perovskite Phosphor. *Chem. Mater.* **2019**, *31* (5), 1738−1744.
(5) Li, M.-R.; Retuerto, M.; Deng, Z.; Stephens, P. W.; Croft, M.; Huang, Q.; Wu, H.; Deng, X.; Kotliar, G.; Sánchez-Benítez, J.; Hadermann, J.; Walker, D.; Greenblatt, M. Giant Magnetoresistance in the Half-Metallic Double-Perovskite Ferrimagnet Mn2FeReO6. *Angew. Chem., Int. Ed.* **2015**, *54* (41), 12069−12073.
(6) Cai, B.; Chen, X.; Xie, M.; Zhang, S.; Liu, X.; Yang, J.; Zhou, W.; Guo, S.; Zeng, H. A Class of Pb-Free Double Perovskite Halide Semiconductors with Intrinsic Ferromagnetism, Large Spin Splitting and High Curie Temperature. *Mater. Horiz.* **2018**, *5* (5), 961−968.
(7) Zhao, X.-G.; Yang, D.; Sun, Y.; Li, T.; Zhang, L.; Yu, L.; Zunger, A. Cu−In Halide Perovskite Solar Absorbers. *J. Am. Chem. Soc.* **2017**, *139* (19), 6718−6725.
(8) McClure, E. T.; Ball, M. R.; Windl, W.; Woodward, P. M. Cs2AgBiX6 (X = Br, Cl): New Visible Light Absorbing, Lead-Free Halide Perovskite Semiconductors. *Chem. Mater.* **2016**, *28* (5), 1348−1354.
(9) Volonakis, G.; Haghighirad, A. A.; Milot, R. L.; Sio, W. H.; Filip, M. R.; Wenger, B.; Johnston, M. B.; Herz, L. M.; Snaith, H. J.; Giustino, F. Cs2InAgCl6: A New Lead-Free Halide Double Perovskite with Direct Band Gap. *J. Phys. Chem. Lett.* **2017**, *8* (4), 772−778.
(10) Greul, E.; Petrus, M. L.; Binek, A.; Docampo, P.; Bein, T. Highly Stable, Phase Pure Cs2AgBiBr6 Double Perovskite Thin Films for Optoelectronic Applications. *J. Mater. Chem. A* **2017**, *5* (37), 19972−19981.
(11) Slavney, A. H.; Leppert, L.; SaldivarValdes, A.; Bartesaghi, D.; Savenije, T. J.; Neaton, J. B.; Karunadasa, H. I. Small-Band-Gap Halide Double Perovskites. *Angew. Chem., Int. Ed.* **2018**, *57* (39), 12765−12770.
(12) Deng, W.; Deng, Z.-Y.; He, J.; Wang, M.; Chen, Z.-X.; Wei, S.-H.; Feng, H.-J. Synthesis of Cs2AgSbCl6 and Improved Optoelectronic Properties of Cs2AgSbCl6/TiO2 Heterostructure Driven by the Interface Effect for Lead-Free Double Perovskites Solar Cells. *Appl. Phys. Lett.* **2017**, *111* (15), 151602.
(13) Bartel, C. J.; Sutton, C.; Goldsmith, B. R.; Ouyang, R.; Musgrave, C. B.; Ghiringhelli, L. M.; Scheffler, M. New Tolerance Factor to Predict the Stability of Perovskite Oxides and Halides. *Science advances* **2019**, *5* (2), No. eaav0693.
(14) Hellenbrandt, M. The Inorganic Crystal Structure Database (ICSD)—Present and Future. *Crystallogr. Rev.* **2004**, *10* (1), 17−22.
(15) Filip, M. R.; Giustino, F. The Geometric Blueprint of Perovskites. *Proc. Natl. Acad. Sci. U. S. A.* **2018**, *115* (21), 5397−5402.
(16) Filip, M. R.; Liu, X.; Miglio, A.; Hautier, G.; Giustino, F. Phase Diagrams and Stability of Lead-Free Halide Double Perovskites Cs2BB′X6: B = Sb and Bi, B′ = Cu, Ag, and Au, and X = Cl, Br, and I. *J. Phys. Chem. C* **2018**, *122* (1), 158−170.
(17) Cai, Y.; Xie, W.; Teng, Y. T.; Harikesh, P. C.; Ghosh, B.; Huck, P.; Persson, K. A.; Mathews, N.; Mhaisalkar, S. G.; Sherburne, M.; Asta, M. High-Throughput Computational Study of Halide Double Perovskite Inorganic Compounds. *Chem. Mater.* **2019**, *31* (15), 5392−5401.
(18) Jain, A.; Voznyy, O.; Sargent, E. H. High-Throughput Screening of Lead-Free Perovskite-like Materials for Optoelectronic Applications. *J. Phys. Chem. C* **2017**, *121* (13), 7183−7187.
(19) Zhao, X.-G.; Yang, J.-H.; Fu, Y.; Yang, D.; Xu, Q.; Yu, L.; Wei, S.-H.; Zhang, L. Design of Lead-Free Inorganic Halide Perovskites for Solar Cells via Cation-Transmutation. *J. Am. Chem. Soc.* **2017**, *139* (7), 2630−2638.
(20) Hedin, L.; Lundqvist, S. Effects of Electron-Electron and Electron-Phonon Interactions on the One-Electron States of Solids. In *Solid State Physics*; Seitz, F., Turnbull, D., Ehrenreich, H., Eds.; Academic Press: 1970; Vol. 23, pp 1−181. DOI: 10.1016/S0081-1947(08)60615-3.
(21) Hedin, L. New Method for Calculating the One-Particle Green's Function with Application to the Electron-Gas Problem. *Phys. Rev.* **1965**, *139* (3A), A796−A823.
(22) Hybertsen, M. S.; Louie, S. G. Electron Correlation in Semiconductors and Insulators: Band Gaps and Quasiparticle Energies. *Phys. Rev. B: Condens. Matter Mater. Phys.* **1986**, *34* (8), 5390−5413.
(23) Albrecht, S.; Reining, L.; Del Sole, R.; Onida, G. Ab Initio Calculation of Excitonic Effects in the Optical Spectra of Semiconductors. *Phys. Rev. Lett.* **1998**, *80* (20), 4510−4513.
(24) Rohlfing, M.; Louie, S. G. Electron-Hole Excitations in Semiconductors and Insulators. *Phys. Rev. Lett.* **1998**, *81* (11), 2312−2315.
(25) Benedict, L. X.; Shirley, E. L.; Bohn, R. B. Optical Absorption of Insulators and the Electron-Hole Interaction: An Ab Initio Calculation. *Phys. Rev. Lett.* **1998**, *80* (20), 4514−4517.
(26) Roessler, D. M.; Walker, W. C. Electronic Spectra of Crystalline NaCl and KCl. *Phys. Rev.* **1968**, *166* (3), 599−606.
(27) Jiang, Z.; Li, Y.; Duan, W.; Zhang, S. Half-Excitonic Insulator: A Single-Spin Bose−Einstein Condensate. *Phys. Rev. Lett.* **2019**, *122* (23), 236402.
(28) Feierabend, M.; Berghäuser, G.; Knorr, A.; Malic, E. Proposal for Dark Exciton Based Chemical Sensors. *Nat. Commun.* **2017**, *8* (1), 14776.
(29) Feierabend, M.; Khatibi, Z.; Berghäuser, G.; Malic, E. Dark Exciton Based Strain Sensing in Tungsten-Based Transition Metal Dichalcogenides. *Phys. Rev. B: Condens. Matter Mater. Phys.* **2019**, *99* (19), 195454.
(30) Schwartz, I.; Schmidgall, E. R.; Gantz, L.; Cogan, D.; Bordo, E.; Don, Y.; Zielinski, M.; Gershoni, D. Deterministic Writing and Control of the Dark Exciton Spin Using Single Short Optical Pulses. *Phys. Rev. X* **2015**, *5* (1), 011009.
(31) Unuchek, D.; Ciarrocchi, A.; Avsar, A.; Watanabe, K.; Taniguchi, T.; Kis, A. Room-Temperature Electrical Control of Exciton Flux in a van Der Waals Heterostructure. *Nature* **2018**, *560* (7718), 340−344.
(32) Bartel, C. J.; Weimer, A. W.; Lany, S.; Musgrave, C. B.; Holder, A. M. The Role of Decomposition Reactions in Assessing First-Principles Predictions of Solid Stability. *npj Computational Materials* **2019**, *5* (1), 4.
(33) Jain, A.; Ong, S. P.; Hautier, G.; Chen, W.; Richards, W. D.; Dacek, S.; Cholia, S.; Gunter, D.; Skinner, D.; Ceder, G.; Persson, K. A. Commentary: The Materials Project: A Materials Genome Approach to Accelerating Materials Innovation. *APL Mater.* **2013**, *1* (1), 011002.
(34) Sun, J.; Ruzsinszky, A.; Perdew, J. P. Strongly Constrained and Appropriately Normed Semilocal Density Functional. *Phys. Rev. Lett.* **2015**, *115* (3), 036402.
(35) Bartel, C. J.; Millican, S. L.; Deml, A. M.; Rumptz, J. R.; Tumas, W.; Weimer, A. W.; Lany, S.; Stevanoví, V.; Musgrave, C. B.; Holder, A. M. Physical Descriptor for the Gibbs Energy of Inorganic Crystalline Solids and Temperature-Dependent Materials Chemistry. *Nat. Commun.* **2018**, *9* (1), 4168.
(36) Ye, W.; Chen, C.; Wang, Z.; Chu, I.-H.; Ong, S. P. Deep Neural Networks for Accurate Predictions of Crystal Stability. *Nat. Commun.* **2018**, *9* (1), 3800.

https://dx.doi.org/10.1021/jacs.9b12440
J. Am. Chem. Soc. 2020, 142, 5135−5145

(37) Sun, W.; Dacek, S. T.; Ong, S. P.; Hautier, G.; Jain, A.; Richards, W. D.; Gamst, A. C.; Persson, K. A.; Ceder, G. The Thermodynamic Scale of Inorganic Crystalline Metastability. *Sci. Adv.* **2016**, *2* (11), No. e1600225.
(38) Heyd, J.; Scuseria, G. E.; Ernzerhof, M. Hybrid Functionals Based on a Screened Coulomb Potential. *J. Chem. Phys.* **2003**, *118* (18), 8207−8215.
(39) Sun, J.; Wu, J.; Tong, X.; Lin, F.; Wang, Y.; Wang, Z. M. Organic/Inorganic Metal Halide Perovskite Optoelectronic Devices beyond Solar Cells. *Advanced Science* **2018**, *5* (5), 1700780.
(40) Kamat, P. V.; Bisquert, J.; Buriak, J. Lead-Free Perovskite Solar Cells. *ACS Energy Letters* **2017**, *2* (4), 904−905.
(41) Zhang, G.; Liu, G.; Wang, L.; Irvine, J. T. S. Inorganic Perovskite Photocatalysts for Solar Energy Utilization. *Chem. Soc. Rev.* **2016**, *45* (21), 5951−5984.
(42) Lufaso, M. W.; Woodward, P. M. Jahn-Teller Distortions, Cation Ordering and Octahedral Tilting in Perovskites. *Acta Crystallogr., Sect. B: Struct. Sci.* **2004**, *60* (1), 10−20.
(43) Shirane, G.; Danner, H.; Pepinsky, R. Neutron Diffraction Study of Orthorhombic BaTiO3. *Phys. Rev.* **1957**, *105* (3), 856−860.
(44) Woodward, P. Octahedral Tilting in Perovskites. I. Geometrical Considerations. *Acta Crystallogr., Sect. B: Struct. Sci.* **1997**, *53* (1), 32−43.
(45) Sun, Q.; Yin, W.-J. Thermodynamic Stability Trend of Cubic Perovskites. *J. Am. Chem. Soc.* **2017**, *139* (42), 14905−14908.
(46) Schmidt, J.; Shi, J.; Borlido, P.; Chen, L.; Botti, S.; Marques, M. A. L. Predicting the Thermodynamic Stability of Solids Combining Density Functional Theory and Machine Learning. *Chem. Mater.* **2017**, *29* (12), 5090−5103.
(47) Faber, F. A.; Lindmaa, A.; von Lilienfeld, O. A.; Armiento, R. Machine Learning Energies of 2 Million Elpasolite ABC2D6 Crystals. *Phys. Rev. Lett.* **2016**, *117* (13), 135502.
(48) Xie, T.; Grossman, J. C. Crystal Graph Convolutional Neural Networks for an Accurate and Interpretable Prediction of Material Properties. *Phys. Rev. Lett.* **2018**, *120* (14), 145301.
(49) Hoye, R. L. Z.; Schulz, P.; Schelhas, L. T.; Holder, A. M.; Stone, K. H.; Perkins, J. D.; Vigil-Fowler, D.; Siol, S.; Scanlon, D. O.; Zakutayev, A.; Walsh, A.; Smith, I. C.; Melot, B. C.; Kurchin, R. C.; Wang, Y.; Shi, J.; Marques, F. C.; Berry, J. J.; Tumas, W.; Lany, S.; Stevanoví, V.; Toney, M. F.; Buonassisi, T. Perovskite-Inspired Photovoltaic Materials: Toward Best Practices in Materials Characterization and Calculations. *Chem. Mater.* **2017**, *29* (5), 1964−1988.
(50) Varignon, J.; Bibes, M.; Zunger, A. Mott Gapping in 3d ABO3 Perovskites without Mott-Hubbard Interelectronic Repulsion Energy U. *Phys. Rev. B: Condens. Matter Mater. Phys.* **2019**, *100* (3), 035119.
(51) Yang, Z.; Peng, H.; Sun, J.; Perdew, J. P. More Realistic Band Gaps from Meta-Generalized Gradient Approximations: Only in a Generalized Kohn-Sham Scheme. *Phys. Rev. B: Condens. Matter Mater. Phys.* **2016**, *93* (20), 205205.
(52) Xu, J.; Liu, J.-B.; Liu, B.-X.; Huang, B. Intrinsic Defect Physics in Indium-Based Lead-Free Halide Double Perovskites. *J. Phys. Chem. Lett.* **2017**, *8* (18), 4391−4396.
(53) Xiao, Z.; Meng, W.; Wang, J.; Mitzi, D. B.; Yan, Y. Searching for Promising New Perovskite-Based Photovoltaic Absorbers: The Importance of Electronic Dimensionality. *Mater. Horiz.* **2017**, *4* (2), 206−216.
(54) Perdew, J. P.; Burke, K.; Ernzerhof, M. Generalized Gradient Approximation Made Simple. *Phys. Rev. Lett.* **1996**, *77* (18), 3865−3868.
(55) Mueller, T.; Malic, E. Exciton Physics and Device Application of Two-Dimensional Transition Metal Dichalcogenide Semiconductors. *npj 2D Materials and Applications* **2018**, *2* (1), 29.
(56) Smith, M. D.; Connor, B. A.; Karunadasa, H. I. Tuning the Luminescence of Layered Halide Perovskites. *Chem. Rev.* **2019**, *119* (5), 3104−3139.
(57) Webster, R.; Bernasconi, L.; Harrison, N. M. Optical Properties of Alkali Halide Crystals from All-Electron Hybrid TD-DFT Calculations. *J. Chem. Phys.* **2015**, *142* (21), 214705.
(58) Rohlfing, M.; Louie, S. G. Electron-Hole Excitations and Optical Spectra from First Principles. *Phys. Rev. B: Condens. Matter Mater. Phys.* **2000**, *62* (8), 4927−4944.
(59) Folkerts, W.; Haas, C. Effect of Exchange Interactions on Gamma Excitons in Transition-Metal Halides. *Phys. Rev. B: Condens. Matter Mater. Phys.* **1985**, *32* (4), 2559−2567.
(60) Deringer, V. L.; Tchougréeff, A. L.; Dronskowski, R. Crystal Orbital Hamilton Population (COHP) Analysis As Projected from Plane-Wave Basis Sets. *J. Phys. Chem. A* **2011**, *115* (21), 5461−5466.
(61) KüPers, M.; Konze, P. M.; Maintz, S.; Steinberg, S.; Mio, A. M.; Cojocaru-Mirédin, O.; Zhu, M.; Müller, M.; Luysberg, M.; Mayer, J.; Wuttig, M.; Dronskowski, R. Unexpected Ge−Ge Contacts in the Two-Dimensional Ge4Se3Te Phase and Analysis of Their Chemical Cause with the Density of Energy (DOE) Function. *Angew. Chem., Int. Ed.* **2017**, *56* (34), 10204−10208.
(62) Henkelman, G.; Arnaldsson, A.; Jónsson, H. A Fast and Robust Algorithm for Bader Decomposition of Charge Density. *Comput. Mater. Sci.* **2006**, *36* (3), 354−360.
(63) Kresse, G.; Furthmüller, J. Efficiency of Ab-Initio Total Energy Calculations for Metals and Semiconductors Using a Plane-Wave Basis Set. *Comput. Mater. Sci.* **1996**, *6* (1), 15−50.
(64) Kresse, G.; Furthmüller, J. Efficient Iterative Schemes for Ab Initio Total-Energy Calculations Using a Plane-Wave Basis Set. *Phys. Rev. B: Condens. Matter Mater. Phys.* **1996**, *54* (16), 11169−11186.
(65) Kresse, G.; Joubert, D. From Ultrasoft Pseudopotentials to the Projector Augmented-Wave Method. *Phys. Rev. B: Condens. Matter Mater. Phys.* **1999**, *59* (3), 1758−1775.
(66) Blöchl, P. E. Projector Augmented-Wave Method. *Phys. Rev. B: Condens. Matter Mater. Phys.* **1994**, *50* (24), 17953−17979.
(67) Giannozzi, P.; Andreussi, O.; Brumme, T.; Bunau, O.; Nardelli, M. B.; Calandra, M.; Car, R.; Cavazzoni, C.; Ceresoli, D.; Cococcioni, M.; Colonna, N.; Carnimeo, I.; Corso, A. D.; Gironcoli, S. de; Delugas, P.; DiStasio, R. A., Jr.; Ferretti, A.; Floris, A.; Fratesi, G.; Fugallo, G.; Gebauer, R.; Gerstmann, U.; Giustino, F.; Gorni, T.; Jia, J.; Kawamura, M.; Ko, H. Y.; Kokalj, A.; Küçükbenli, E.; Lazzeri, M.; Marsili, M.; Marzari, N.; Mauri, F.; Nguyen, N. L.; Nguyen, H. V.; Otero-de-la-Roza, A.; Paulatto, L.; Poncé, S.; Rocca, D.; Sabatini, R.; Santra, B.; Schlipf, M.; Seitsonen, A. P.; Smogunov, A.; Timrov, I.; Thonhauser, T.; Umari, P.; Vast, N.; Wu, X.; Baroni, S. Advanced Capabilities for Materials Modelling with Quantum ESPRESSO. *J. Phys.: Condens. Matter* **2017**, *29* (46), 465901.
(68) Giannozzi, P.; Baroni, S.; Bonini, N.; Calandra, M.; Car, R.; Cavazzoni, C.; Ceresoli, D.; Chiarotti, G. L; Cococcioni, M.; Dabo, I.; Dal Corso, A.; de Gironcoli, S.; Fabris, S.; Fratesi, G.; Gebauer, R.; Gerstmann, U.; Gougoussis, C.; Kokalj, A.; Lazzeri, M.; Martin-Samos, L.; Marzari, N.; Mauri, F.; Mazzarello, R.; Paolini, S.; Pasquarello, A.; Paulatto, L.; Sbraccia, C.; Scandolo, S.; Sclauzero, G.; Seitsonen, A. P; Smogunov, A.; Umari, P.; Wentzcovitch, R. M QUANTUM ESPRESSO: A Modular and Open-Source Software Project for Quantum Simulations of Materials. *J. Phys.: Condens. Matter* **2009**, *21* (39), 395502.
(69) Hamann, D. R. Optimized Norm-Conserving Vanderbilt Pseudopotentials. *Phys. Rev. B: Condens. Matter Mater. Phys.* **2013**, *88* (8), 085117.
(70) Schlipf, M.; Gygi, F. Optimization Algorithm for the Generation of ONCV Pseudopotentials. *Comput. Phys. Commun.* **2015**, *196*, 36−44.
(71) Deslippe, J.; Samsonidze, G.; Strubbe, D. A.; Jain, M.; Cohen, M. L.; Louie, S. G. BerkeleyGW: A Massively Parallel Computer Package for the Calculation of the Quasiparticle and Optical Properties of Materials and Nanostructures. *Comput. Phys. Commun.* **2012**, *183* (6), 1269−1289.
(72) Deslippe, J.; Samsonidze, G.; Jain, M.; Cohen, M. L.; Louie, S. G. Coulomb-Hole Summations and Energies for GW Calculations with Limited Number of Empty Orbitals: A Modified Static Remainder Approach. *Phys. Rev. B: Condens. Matter Mater. Phys.* **2013**, *87* (16), 165124.

https://dx.doi.org/10.1021/jacs.9b12440
J. Am. Chem. Soc. 2020, 142, 5135−5145

(73) Hinuma, Y.; Pizzi, G.; Kumagai, Y.; Oba, F.; Tanaka, I. Band Structure Diagram Paths Based on Crystallography. *Comput. Mater. Sci.* **2017**, *128*, 140−184.
(74) Berger, R. F.; Neaton, J. B. Computational Design of Low-Band-Gap Double Perovskites. *Phys. Rev. B: Condens. Matter Mater. Phys.* **2012**, *86* (16), 165211.
(75) King, G.; Woodward, P. M. Cation Ordering in Perovskites. *J. Mater. Chem.* **2010**, *20* (28), 5785−5796.
(76) Ong, S. P.; Richards, W. D.; Jain, A.; Hautier, G.; Kocher, M.; Cholia, S.; Gunter, D.; Chevrier, V. L.; Persson, K. A.; Ceder, G. Python Materials Genomics (Pymatgen): A Robust, Open-Source Python Library for Materials Analysis. *Comput. Mater. Sci.* **2013**, *68*, 314−319.
(77) Maintz, S.; Deringer, V. L.; Tchougréeff, A. L.; Dronskowski, R. LOBSTER: A Tool to Extract Chemical Bonding from Plane-Wave Based DFT. *J. Comput. Chem.* **2016**, *37* (11), 1030−1035.

https://dx.doi.org/10.1021/jacs.9b12440
J. Am. Chem. Soc. 2020, 142, 5135−5145